Progress In Electromagnetics Research C, Vol. 138, 91–104, 2023

Sub-6 GHz Metallic via Integrated MIMO Antenna Array for 5G Smartphone

Inderpreet Kaur[1], Banani Basu[2, *], and Anil K. Singh[3]

Abstract—A miniaturized and closely packed eight element annular ring multiple-input multiple-output (MIMO) antenna array is designed to operate from the 3 to 6 GHz band for 5G smartphone applications. In MIMO, the orthogonally placed antenna pairs maintain high isolation. The proposed decoupling structures placed between two adjacent antenna pairs improve the isolation. The decoupling structure consists of a rectangular metallic strip with metallic vias that reduces the mutual coupling and excites the additional modes to extend the bandwidth from 3 to 6 GHz. The MIMO structure offers isolation of more than 24 dB, ECC of less than 0.1, TARC of less than 7 dB over the complete operation band, DG of 10 dB, and more than 95% efficiency. The specific absorption rates (SARs) of the antenna placed in the human head and hand models are 0.41 W/kg and 0.66 W/kg, respectively. The performance obtained with the fabricated prototype offers excellent matching with that of the simulated ones.

1. INTRODUCTION

MIMO technology has been found crucial for 5G smartphones. However, as multiple antennas are packed into a smartphone's limited area, antenna elements become densely linked, resulting in low isolation, reduced antenna efficiency, and high SAR values. In recent years, there has been a growing demand for compact-sized antennas with enhanced bandwidth and an increased number of ports in various wireless communication applications. The isolation between ports has emerged as a crucial parameter for achieving optimal performance. However, achieving high isolation while maintaining the compactness of the antenna remains a significant challenge. Several studies have been conducted in the field of antenna design to address these requirements. There exist several approaches that can help increase isolation [1–15]. A neutralization line presented in [1–3], a common ground plane technique reported in [4, 5], and a gap-coupled feeding arrangement adopted in [6, 7] are the methods employed to mitigate the mutual coupling. Due to smaller size, the structures have limited impedance bandwidth, which is insufficient to cover the requisite operating bands. A T-shaped ground stub along with a split U-shaped stub connected to the radiating elements has been used in [8] to improve the isolation and impedance bandwidth. [9] has proposed a parasitic strip and defected ground structure with engraving slits on the ground to achieve broadband and good isolation. In [10], two G-shaped elements in the upper layer and two inverted L protruding branches and a T slot etched in the ground have been utilized to reduce the mutual coupling. [11] has presented a 4-port MIMO antenna with diamond-shaped slots and a defective ground structure for 5G applications. The article [12] has described a hybrid loop/open-slot antenna to excite additional modes for an LTE smartphone application. The eight off-centred fed modified rectangular open-loop resonating radiators with circular polarization (CP) behaviour have

Received 1 June 2023, Accepted 13 September 2023, Scheduled 3 October 2023

* Corresponding author: Banani Basu (banani@ece.nits.ac.in).

[1] Department of Electronics & Communication Engineering, MJPRU Bareilly, Uttar Pradesh, India. [2] Department of Electronics & Communication Engineering, NIT Silchar, Assam, India. [3] Department of Electronics & Instrumentation Engineering, MJPRU Bareilly, Uttar Pradesh, India.

been realised by utilising a narrow slit on the loop and a modified ground plane [13]. A high-isolation printed eight-element array operating at 3.45 GHz (3.3–3.6 GHz) has been investigated in [14]. The array elements are placed on the side-edge of the frame symmetrically, to achieve good isolation by employing hybrid decoupling structures [15]. Low correlation and high isolation are the fundamental requirements for MIMO systems. [16] has employed a decoupling technique, via embedded metallic strips, to enhance the isolation and extend the bandwidth. The number of antenna elements in a MIMO system increases data rates and channel capacity. However, as the number of elements increases, so does the overall system's complexity, due to the increasing correlation among elements. As a result, low correlation and high isolation are fundamental requirements for MIMO systems. The proposed work is focused on the design of a compact-sized antenna with enhanced bandwidth and increased port count while prioritizing isolation as the main parameter. The physical dimensions of the proposed 8-element MIMO are $0.81\lambda \times 0.81\lambda$ which is the smallest ever reported. The metallic vias offer an impressive isolation level of more than 20 dB all over the operating band. MIMO arrays employ the new decoupling technique, a via on the metallic strip which not only enhances the isolation but also extends the bandwidth indicating promising advancements in achieving high-performance compact antenna designs. The MIMO antenna system offers bandwidth from 3 to 6 GHz, envelope correlation coefficient (ECC) up to 0.05, total active reflection coefficient (TARC) of -18 dB, and channel capacity loss of 0.4 bits/s/Hz.

2. ANTENNA DESIGN

The number of antenna elements chosen for a MIMO system may vary based on the application, available resources, and system requirements. We have proposed an eight elements MIMO antenna array to achieve substantially improved channel capacity, reliability, interference mitigation, and spatial processing capabilities. We have designed the three 2-element MIMO arrays, namely Models I, II, and III, and subsequently presented the models in Figs. 1(a), (b), and (c), respectively. Model I comprises two circular patches of radius $r1$ with a microstrip feed etched on FR4 having a permittivity of 4.4. The corresponding S_{11}, S_{22}, and S_{12} values are presented in Figs. 1(d), (e), (f), indicating poor impedance matching and inadequate isolation. So, Model II, the ring antenna having outer radius $r1$ and inner radius $r2$, is derived from Model I, which offers distinct improvement in S_{11} with a return loss minimum of -27 dB and low mutual coupling. Next, the ring has been loaded with a slot to further enhance the S_{11} parameter up to -30 dB. This progression in design showcases improved impedance matching and isolation, as shown in Figs. 1(d), (e), (f). Another set of similar antenna pair, including a 2-element slotted ring antenna, has been integrated with Model III. The resulting four-port array is presented in the inset picture of Figs. 2(a) and (b). The corresponding reflection and isolation parameters of the array are presented in Figs. 2(a) and (b). It is seen from Fig. 2(a) that the addition of the two more elements makes the circuit inductive and shifts the resonance towards the right-hand side. Finally, two more pairs are symmetrically added, resulting in an eight ports MIMO array as in Figs. 2(c) and (d) (inset). The simulated reflection coefficients of the 8-port structure are shown in Fig. 2(c). The orthogonal elements in this configuration exhibit good isolation of more than 20 dB without any decoupling structure, as shown in Fig. 2(d). However, the isolation between the adjacent elements still needs improvement. So a metal strip integrated with vias has been placed between the adjacent elements, which bestows substantially improved reflection and Isolation curves as in Figs. 2(e) and (f). The size of the substrate of the 8 ports MIMO is $0.81\lambda \times 0.81\lambda$, and the antennas are fed through the system ground via 50 SubMiniature version A (SMA) connectors. The two identical monopole antennas are placed 14.4 mm away from the centre to centre on the top of the substrate. The partial rectangular ground is interconnected to form a shared ground plane.

2.1. Parametric Studies

In this section, parametric analysis and structure optimization are carried out. $r1$ and $r2$ of the ring are modified to improve the reflection coefficient and isolation. The outer radius of an annular ring is seen to provide flexibility in controlling the resonant frequency over the operating band. S parameters are studied considering different values of $r2$ and $r1$ and are shown in Figs. 3(a) and (b), respectively. It can be seen that the isolation becomes better with the decrease in inner and outer radii as it increases

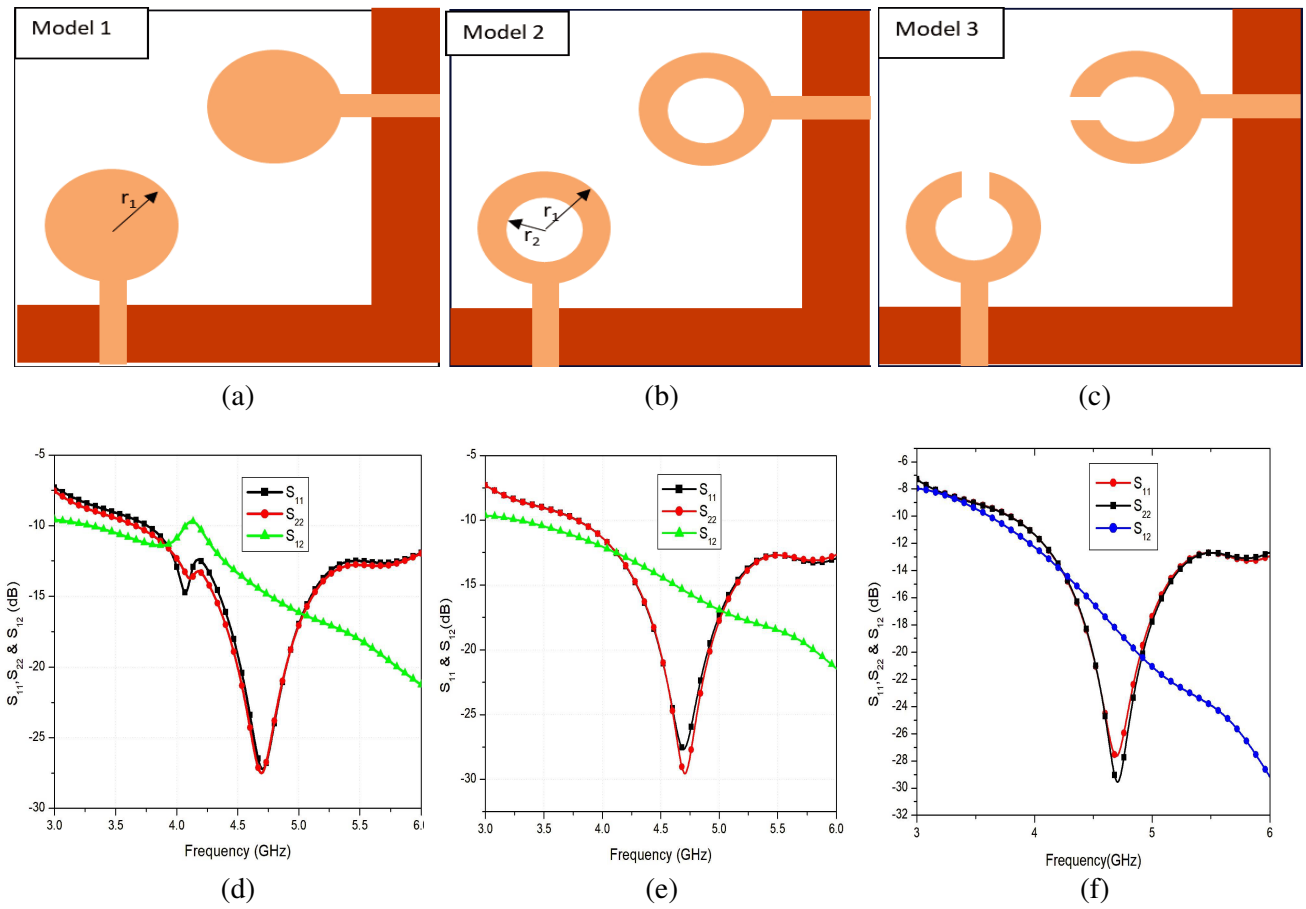

Figure 1. Design steps. (a) Model 1, (b) Model 2, (c) Model 3. Scattering parameter of models. (d) Model 1, (e) Model 2, (f) Model 3.

the gap between elements. The optimized value of '$r1$' is set at 5.5 mm to obtain the desired operating band of 3–6 GHz and optimum isolation. Based on the gain and isolation performance, the optimized $r2$ is set at 2.5 mm. It is noticed that the isolation is enhanced with the increase in thickness of the strip for fixed $r1$ and $r2$ values.

2.2. Decoupling Structure

A lot of decoupling methods have been reported in [17–22]. The study reveals that the isolation is less than 10 dB without decoupling structures as in Figs. 3(a) and (b). Operating band is modified, and isolation is enhanced when the strip of length 26 mm is placed between two adjacent antennas as in Figs. 4(a) and (b). It excites TM21 mode and splits the operating band into two parts: 3–4.1 GHz and 4.2–6 GHz. The metallic vias drilled on the isolating strip cause discontinuities and excite the nearby modes TM21 and TM31 along with TE10 which get merged to improve the bandwidth from 3 to 6 GHz as in Fig. 4(c). Fig. 4(d) shows that the via-enabled metallic strip acts as a wave trapper that traps the radiation to minimize the coupling significantly, at least up to 20 dB all over the band. It is noticed that the isolation is enhanced with the increase in thickness of the strip for fixed $r1$ and $r2$ values. The study has investigated the vector current distribution of the via-enabled structure at 5.6 GHz when half of the ports are excited as shown in Figs. 5(a) and (b). The ground plane current has direction along the x-axis when being fed through the right-side ports 1, 8, 7, and 6 as in Fig. 5(a), but the direction changes when being fed through the left-side ports 2, 3, 5, and 4 as shown in Fig. 5(b). It corroborates the existence of the orthogonal ground current mode that blocks the current coupling through the ground

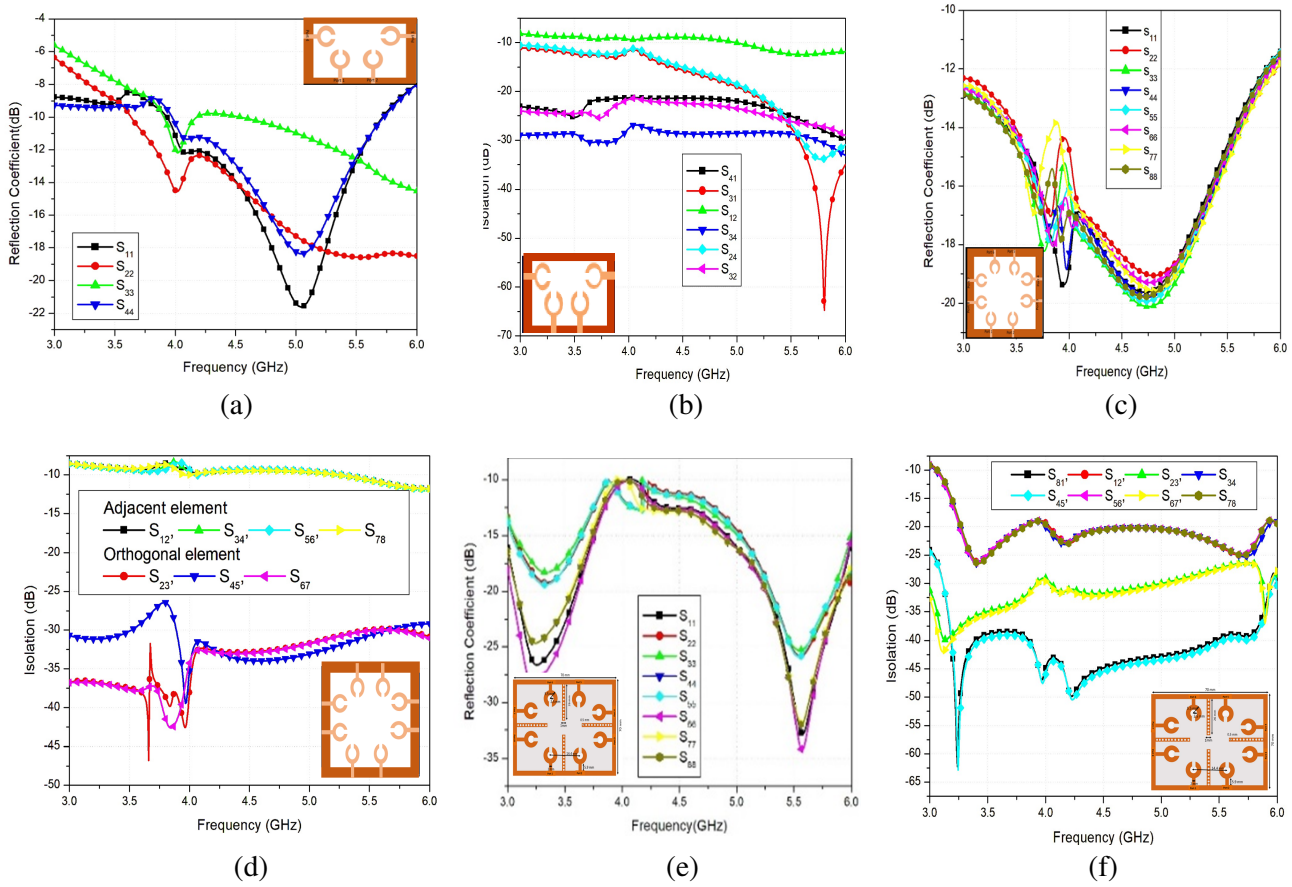

Figure 2. Four element antenna (a) reflection coefficient, (b) isolation, eight element antenna, (c) reflection coefficient, (d) isolation, eight element antenna with strip integrated via, (e) reflection coefficient, (f) isolation.

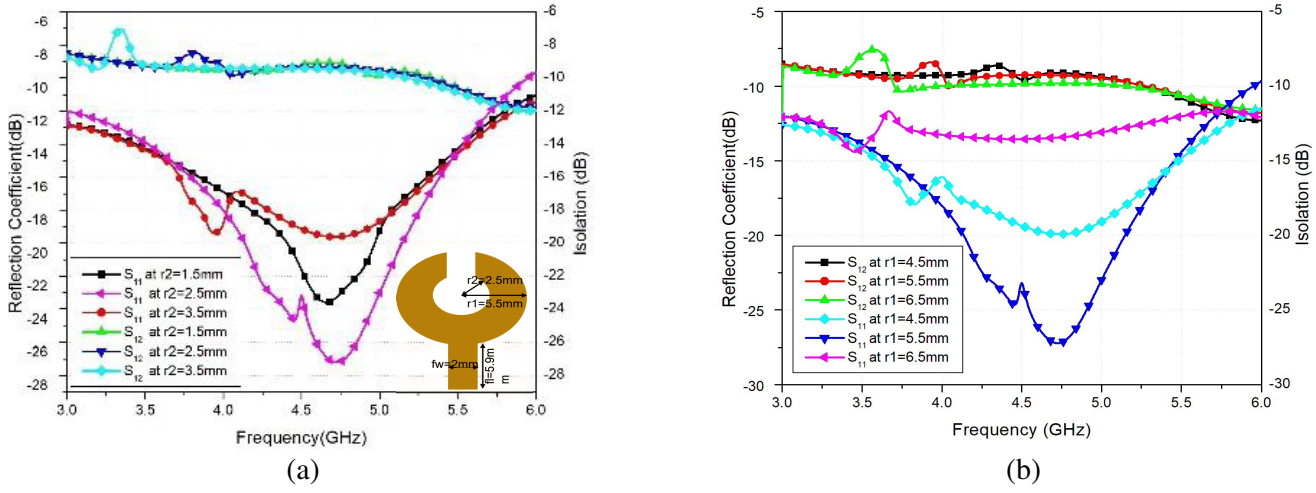

Figure 3. S parameters for different (a) $r2$ at a fixed value of $r1$, (b) $r1$ at a fixed value of $r2$.

plane mitigating the coupling [17]. Figs. 5(c) and (d) reveal the current distribution on the ground plane with metallic strips at 3.4 and 5.6 GHz. The current distributions on the structure at 3.4 GHz and 5.6 GHz with the metallic strips embedded with vias are presented in Figs. 5(e) and (f). We have examined the variation of current distributions on the single antenna pair with and without the wave trap in Figs. 5(g) and (h). It is seen from Figs. 5(g) and (h) that the intensity of current distribution significantly reduces in the presence of wave traps.

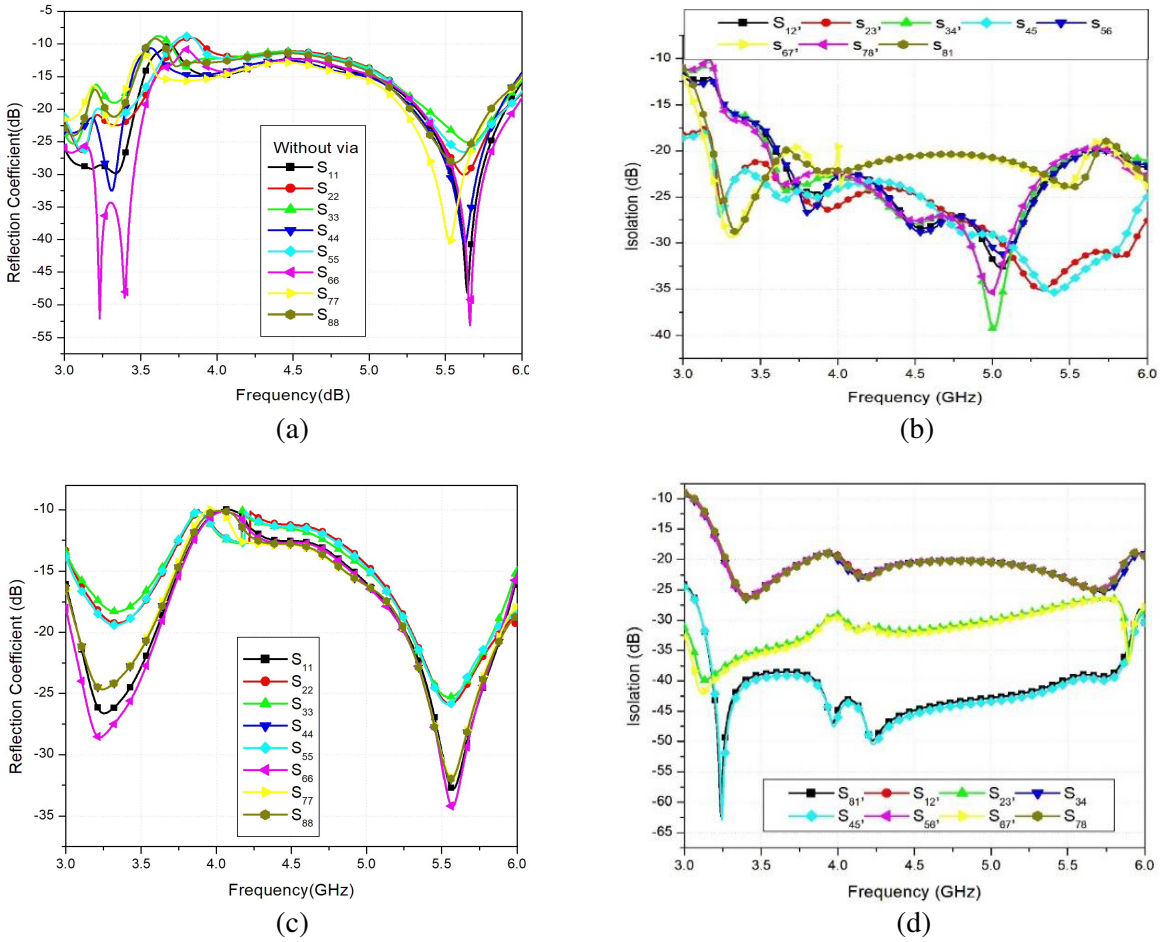

Figure 4. S parameters with metallic strip. (a) Reflection coefficient, (b) isolation and with metallic via integrated strips, (c) reflection coefficient, (d) isolation.

3. RESULTS AND DISCUSSION

Figure 6(a) depicts the top and bottom schematics of the proposed eight-element antenna with an optimized dime. The equivalent circuit of the design is included in Fig. 6(b). The equivalent circuit is the combination of two LC resonant circuits connected in series. Each resonant circuit represents the excitation of a specific mode. The shorting vias presented in the proposed structure contribute to the shunt inductances. When mode 1 or mode 2 is excited, the equivalent inductances $Lv1$, $Lv1$, ..., Lvn due to the shorting vias reduce the total inductance of the resonant circuits, causing a shift in resonant frequencies, which further enhances the operating band. Moreover, the shorting vias stop the propagation of electromagnetic (EM) wave to the adjacent elements and enhance the isolation (Sij) as illustrated in Fig. 7(b). Figs. 6(c) and 6(d) show the bottom and top prototypes of the MIMO antenna.

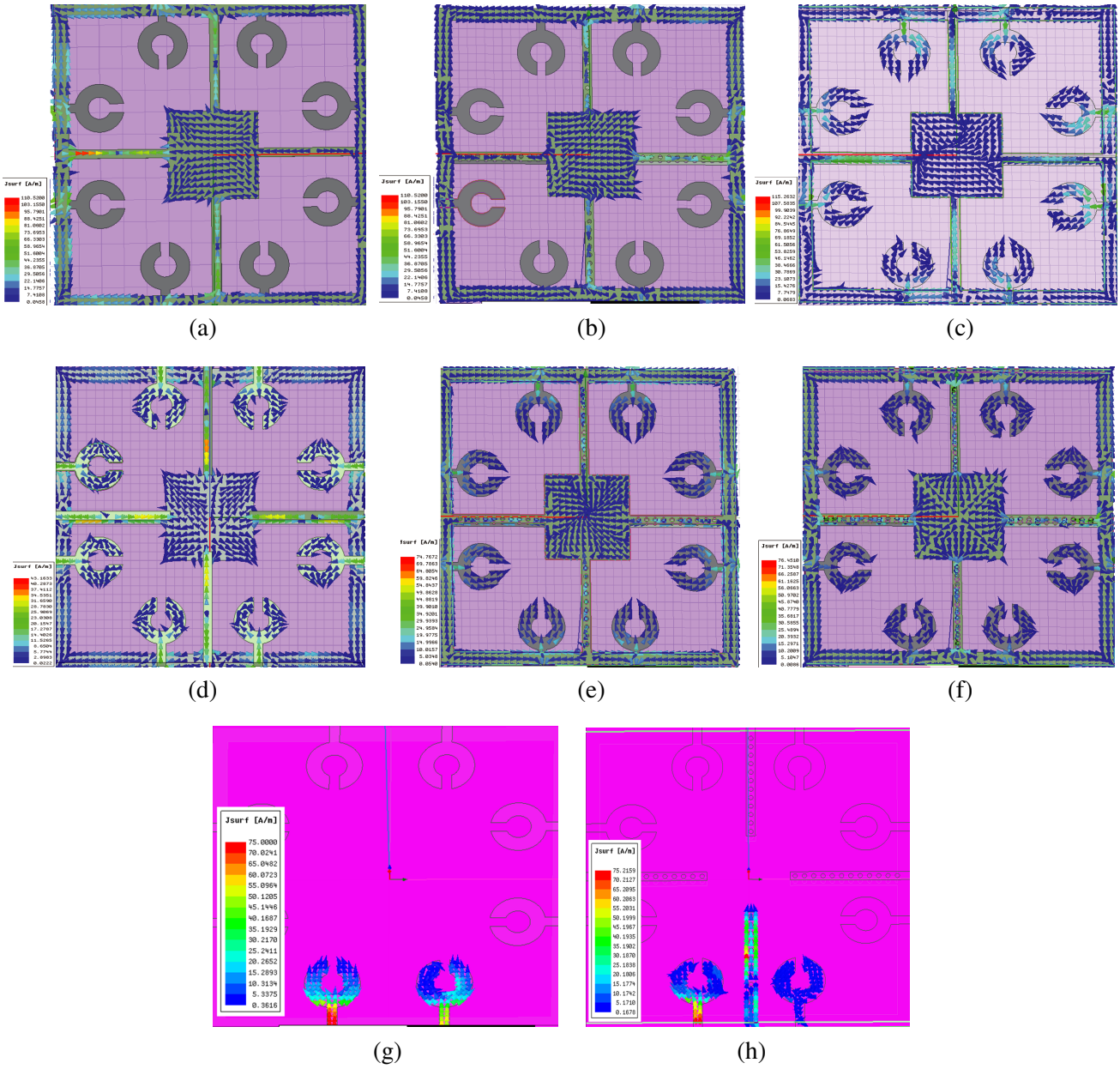

Figure 5. Current distribution on the ground plane (a) when fed through ports 1, 8, 7, 6 at 5.6 GHz, (b) when fed through ports 2, 3, 4, 5 at 5.6 GHz. Fully excited (c) without via array at 3.4 GHz, (d) without via array at 5.6 GHz, (e) with via array at 3.4 GHz, (f) with via at 5.6 GHz. At 3.4 GHz, for single pair (g) without strip, (h) with via integrated strip.

Figures 7(a) and (b) present the measured and simulated reflection coefficients and isolations. Fig. 7(c) presents the gain of the proposed structure measured in the broadside direction at $\theta = 0°$ and $\phi = 0°$. Gain is found as 5 dBi at 3.4 GHz and 7.8 dBi at 5.6 GHz. The gain is less at the lower band because the impedance is capacitive at the low-frequency band. Gain of the proposed MIMO antenna depends on the efficiency and physical aperture of the MIMO antenna which varies with frequency. So, at 4–4.25 GHz, though the efficiency drops at 88%, the gain remained almost stable. The average radiation efficiency is almost 95% shown in Fig. 7(d).

The radiation patterns in E and H fields are presented in Fig. 8. As we use the 8 element

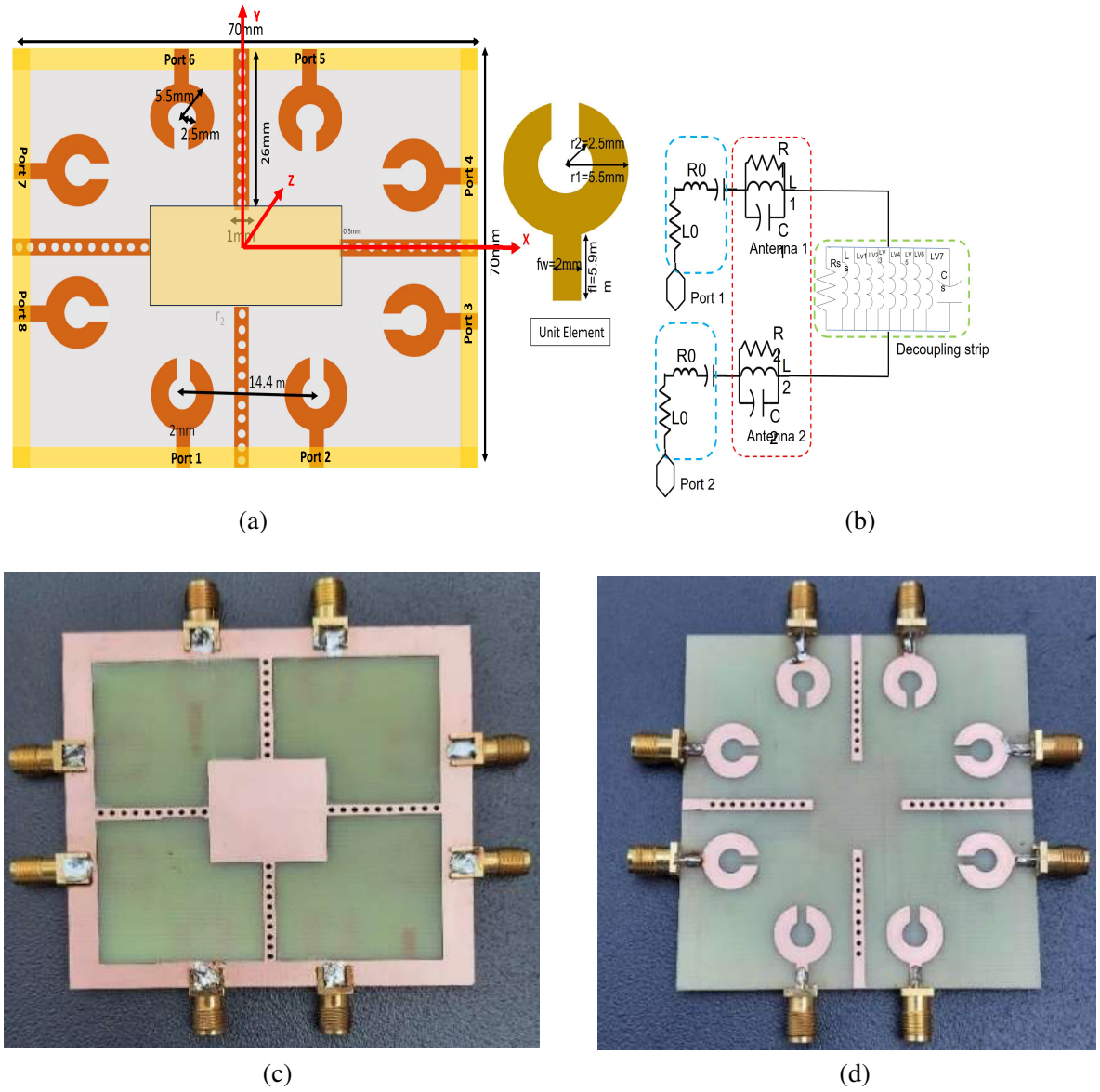

Figure 6. MIMO prototype. (a) Top and bottom schematics of the proposed eight-element antenna. (b) Equivalent circuit prototype. (c) Bottom view. (d) Top view.

antenna array, the main lobe direction is shifted due to the vector addition of E fields caused by the individual antennas. Antennas having equal excitation currents are placed on a rectangular contour which generates an array pattern with a large front-to-back lobe ratio. Fig. 8 describes the Co-P and X-P radiation patterns of the 8-element MIMO antenna at 3.4 GHz and 5.6 GHz. E field patterns ensure reasonable Co-Pole and X-Pole isolation at both the frequencies whereas H field patterns provide 10 dB and 9 dB isolation at 3.4 GHz and 5.6 GHz, respectively. The proposed antenna is linearly polarized. Antenna arrangement in perpendicular position causes higher cross polarization level which reduces the coupling level more significantly.

3.1. MIMO Diversity Analysis

The envelope correlation coefficient (ECC) measures the impact of various radio frequency (RF) signal paths reaching the antenna elements. The simulated value of the ECC of the proposed antenna, as

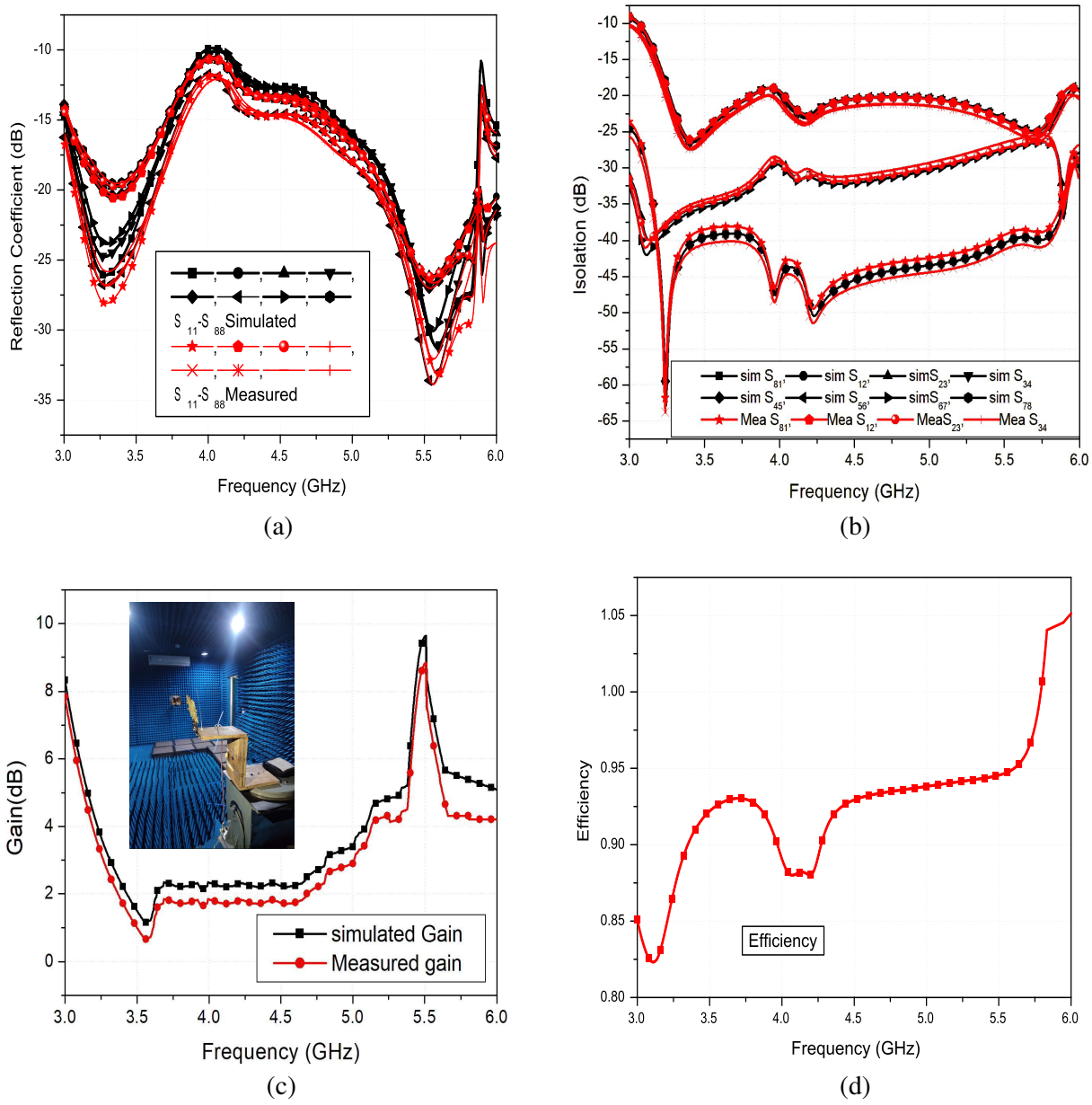

Figure 7. (a) Reflection coefficient. (b) Isolation. (c) Gain. (d) Efficiency.

shown in Fig. 9(a) is less than 0.2 for the complete operating band [23–26], and ρ is calculated using Eq. (1)

$$\mathrm{ECC} = \rho\,(i,j,N) = \frac{\left|\left(\sum_{n=1}^{N} S_{in}^{*} S_{nj}\right)\right|^{2}}{\prod_{k=i,j}\left(1-\sum_{n=1}^{N} S_{kn}^{*} S_{nk}\right)} \tag{1}$$

where $i,\ j$ are any two ports and $N = 8$.

Diversity gain (DG) is mathematically related to ECC and calculated according to Eq. (2). The

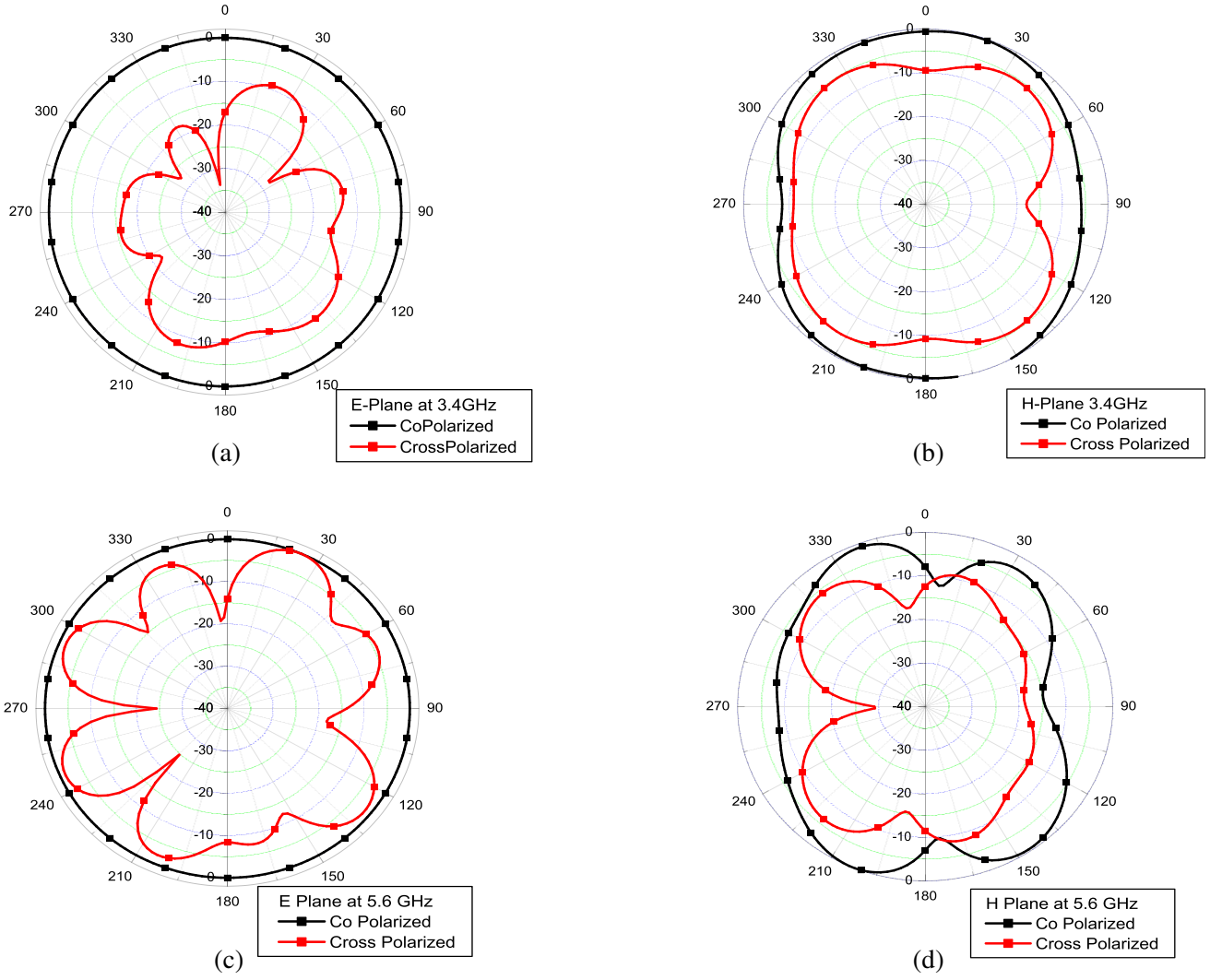

Figure 8. Radiation pattern at 3.4 GHz (a) E-plane, (b) H-plane and at 5.6 GHz (c) E-plane, (d) H-plane.

simulated value of DG is provided in Fig. 9(b).

$$\mathrm{DG} = 10\sqrt{(1 - |\mathrm{ECC}|^2)} \tag{2}$$

Total active reflection coefficient (TARC) is defined as the ratio of the square root of the total reflected power to the square root of the total incident power, which represents the mutual coupling between ports and the combination of random signals [27]. TARC is calculated using Eq. (3).

$$\mathrm{TARC} = \sqrt{\sum_{i}^{8}\left(\sum_{j}^{8}(S_{ij})/2\right)} \tag{3}$$

Figure 9(c) represents the TARC of the proposed array.

The value of Channel Capacity (CC) of the proposed 8 element MIMO is derived using Eq. (4).

$$\mathrm{CC} = E\left[\log_2\left[\det\left(I + \eta\frac{\mathrm{SNR}}{K}HH^H\right)\right]\right] \tag{4}$$

The E is the expectation with respect to different channel realisations, I an identity matrix, η the efficiency, SNR the mean signal-to-noise ratio, K the rank of HH^H where H is the channel matrix,

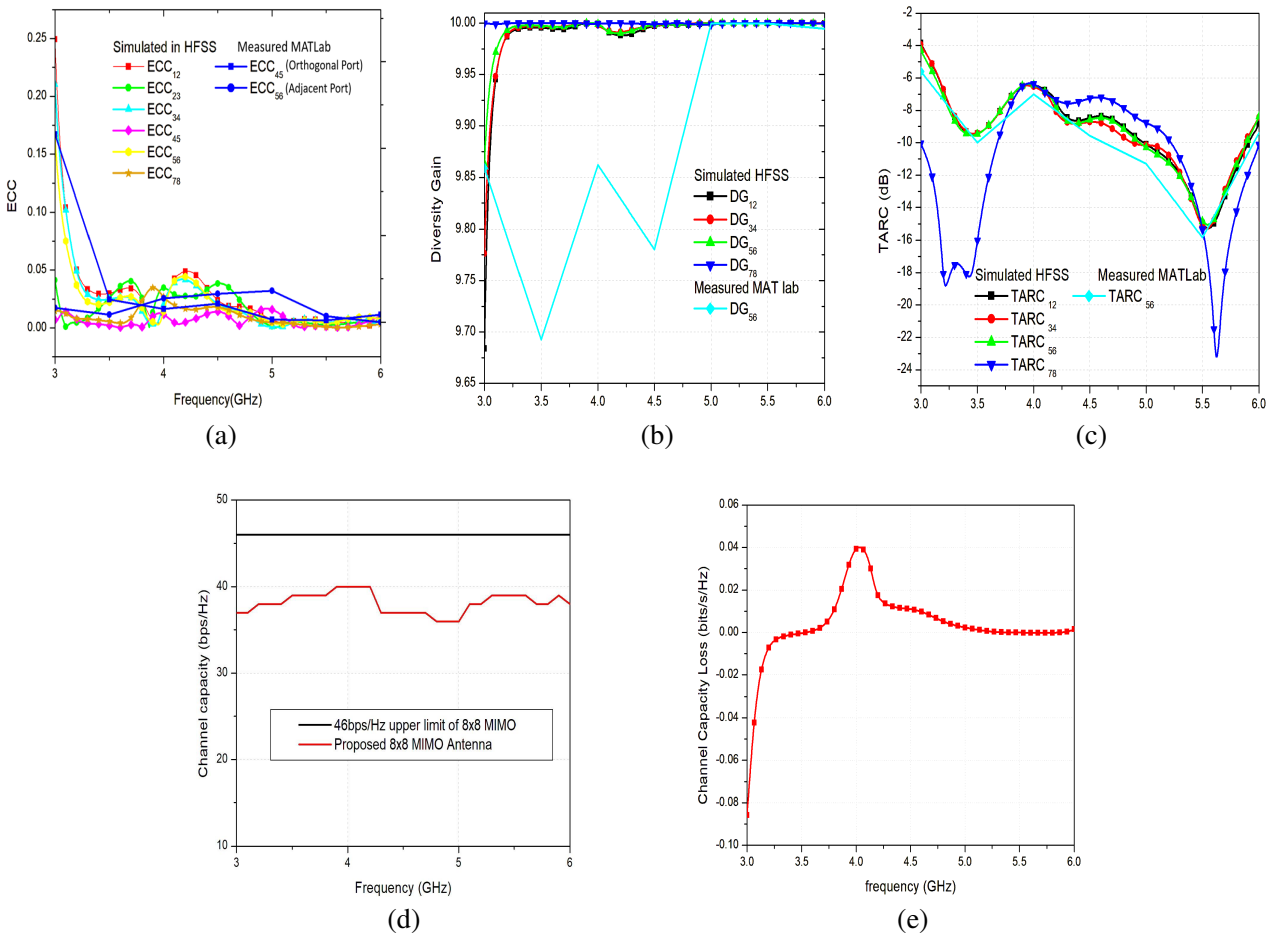

Figure 9. Array parameter. (a) ECC. (b) Diversity gain. (c) TARC. (d) Channel capacity. (e) Channel capacity loss.

and H^H denotes the Hermitian of matrix H [28–31, 38]. The channel capacity of the proposed array is calculated and indicated in Fig. 9(d). The CC value is about 43 bps/Hz considering that the transmitting antennas are uncorrelated (ECC = 0). The ergodic channel capacities are averaged over 10,000 Rayleigh fading realisations with an SNR ratio of 20 dB for eight-antenna array. We know that MIMO antennas allow higher data throughput within a channel. Channel Capacity Loss (CCL) is the maximum data rate at which signal can be transmitted with the least error. For the MIMO antenna, it is desirable that the CCL would lie below 0.4 bps/Hz. The CCL is calculated as per Eq. (5); CCL depends on the *Sii* and *Sij*; and both rise at 4 GHz increasing the CCL at that frequency as in Fig. 9(e).

$$\mathrm{CCL} = \log_2 \det(\psi_R) \tag{5}$$

$$\psi_R = \begin{pmatrix} \psi_{11} & \cdots & \psi_{18} \\ \vdots & \ddots & \vdots \\ \psi_{81} & \cdots & \psi_{88} \end{pmatrix} \tag{6}$$

$$\psi_{ii} = \left(1 - \sum_{i,j=1}^{8} |S_{ij}|^2\right) \psi_{ij} = -\left(S_{ii}^* S_{ij} + S_{ji}^* S_{ij}\right) \tag{7}$$

it ensures that the CCL of the proposed array over the entire band is below the specified level.

3.2. SAR Analysis

To perform the SAR analysis of the MIMO antenna, we utilized [HFSS 19] to model the human body parts and accurately simulate their interaction with the electromagnetic fields generated by the antennas. The software calculates the SAR values for each tissue layer and provides an overall SAR value for the human body. The simulation results have presented that the SAR value for the MIMO antenna is well below the maximum allowable limit of 2 W/kg set by regulatory bodies. The SAR values are found to be 0.41 W/kg for the head at a frequency 3.4 GHz and 0.611 W/kg for the head at a frequency 5.6 GHz over 10-g tissue when it is 2 mm apart from the skin. The SAR value for hand is 0.66 W/kg at 3.4 GHz and 0.557 at 5.6 GHz. SAR is simulated for the upper portion of the handset (ant1, ant2, ant7, ant8), where the antennas are closest to the human head. The SARs for the human head model as well as the human head and hand model combined at 3.4 GHz and 5.6 GHz are shown in Fig. 10 and Table 1. The transmitting power set to flow through the structure is 0.5 W, and the mobile handset is placed at

Table 1. SAR for head and hand model.

	Head SAR			Hand SAR		
Port	I/P Power	Frequency (GHz)	SAR W/kg	I/P Power	Frequency (GHz)	SAR W/kg
Port 1–8	50 mW	3.4	0.41	50 mW	3.4	0.66
Port 1–8	50 mW	5.6	0.611	50 mW	5.6	0.557

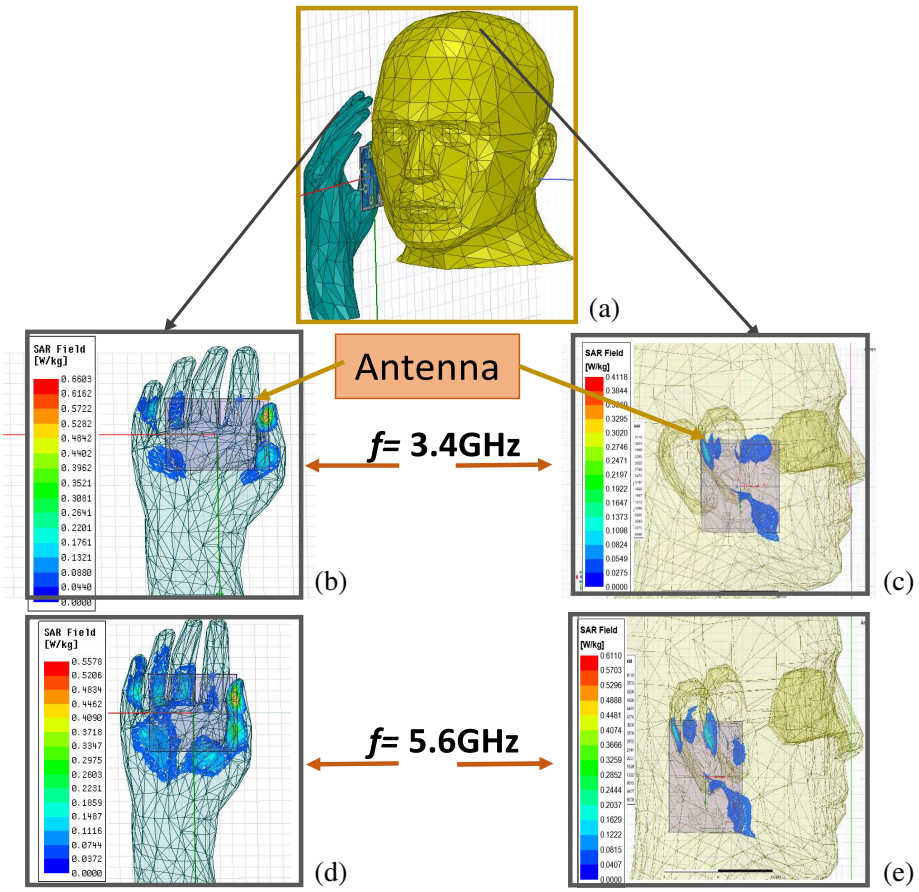

Figure 10. SAR of the proposed MIMO antenna at $\theta = 0°$ and $\phi = 0°$. (a) SAR model at 3.4 GHz. (b) Hand SAR. (c) Head SAR, at 5.6 GHz. (d) Hand SAR. (e) Head SAR.

Table 2. Comparison of proposed work with previously published work.

Ref.	Total size (λ)	No. of Elements	Bandwidth (GHz)	Isolation (dB)	Decoupling Method	ECC	Efficiency
[18]	$2.0 \times 0.98 \times 0.010$	08	4.0–5.6 24–29.5	22	-	-	70%
[19]	$1.7 \times 0.90 \times 0.009$	08	3.4–3.6	17	-	0.05	62–76%
[20]	$1.7 \times 0.90 \times 0.009$	10	3.4–3.6 4.67–6.24	22	-	0.05	65–82%
[21]	$1.7 \times 0.90 \times 0.009$	08	3.4–3.8 5.15–5.925	12	-	0.15	41–82%
[22]	$0.46 \times 0.46 \times 0.079$	04	4.58–6.12	15.4	Decoupling structure	0.15	67–82%
[32]	$1.6 \times 0.77 \times 0.013$	08	3.3–4.2	9.5	-	-	
[33]	$2.2 \times 1.10 \times 0.011$	08	4.4–5.04	18	-	-	
[34]	$2.1 \times 1.03 \times 0.017$	08	4.37–5.5	22	-	-	
Proposed work	$0.81 \times 0.81 \times 0.018$	08	3.5–6	24	Via Array on Metallic strip	0.05	95%

2 mm away from both the head and the hand. The performance of the proposed antenna is compared with that of the previously published works and presented in Table 2.

4. CONCLUSION

The communication demonstrates an 8×8 MIMO system composed of pairs of closely packed antenna elements, which shows good isolation and ECC performance despite the proximity of the elements. A metallic via array is employed as a decoupling structure between adjacent elements and excites the nearby modes to resonate the antenna from 3 to 6 GHz [35–37]. The MIMO antenna exhibits excellent diversity performance, with mutual coupling below 24 dB, diversity gain of 10 dB, and ECC less than 0.05 across the whole band. Moreover, the radiation efficiency of the MIMO system is 95%, and the channel capacities exceed 40 bps/Hz across the operating bands. The SAR value for the head and hand model is below 0.66 W/kg. The proposed MIMO antenna is compact and offers a peak gain of up to 7.8 dBi. The proposed MIMO antenna is a strong 5G smartphone application contender. Furthermore, the gain can be increased by using low dielectric loss material.

REFERENCES

1. Liu, D., M. Zhang, H. Luo, H. Wen, and J. Wang, "Dual-band platform free PIFA for 5G MIMO, application of mobile devices," *IEEE Transactions on Antennas and Propagation*, Vol. 66, No. 11, 6328–6333, 2018. Available: 10.1109/tap.2018.2863109.
2. Shi, X., M. Zhang, S. Xu, D. Liu, H. Wen, and J. Wang, "Dual-band 8-element MIMO antenna with a short neutral line for 5G mobile handset," *2017 11th European Conference on Antennas and Propagation (EUCAP)*, IEEE, Paris, France, 2017. Available: 10.23919/eucap.2017.7928046.
3. Shi, X., M. Zhang, H. Wen, and J. Wang, "Compact quadruple band MIMO antenna for 5G mobile applications," *12th European Conference on Antennas and Propagation (EuCAP 2018)*, IET, London, UK, 2018. Available: 10.1049/cp.2018.0372.
4. Malviya, L., R. Panigrahi, and M. Kartikeyan, "MIMO antennas with diversity and mutual coupling reduction techniques: A review," *International Journal of Microwave and Wireless Technologies*, Vol. 9, No. 8, 1763–1780, 2017. Available: 10.1017/s1759078717000538.

5. Nadeem, I. and D.-Y. Choi, "Study on mutual coupling reduction techniques for MIMO antennas," *IEEE Access*, Vol. 7, 563–586, 2019. Available: 10.1109/access.2018.2885558.
6. Ding, Z., T. Yao, X. Liu, X. Wang, and Z. Liu, "An eight-port dual-band antenna array for 5G smartphone applications," *2018 Cross-Strait Quad-Regional Radio Science and Wireless Technology Conference (CSQRWC)*, IEEE, Xuzhou, China, 2018. Available: 10.1109/csqrwc.2018.8455745.
7. Guo, J., L. Cui, C. Li, and B. Sun, "Side-edge frame printed eight port dual-band antenna array for 5G smartphone applications," *IEEE Transactions on Antennas and Propagation*, Vol. 66, No. 12, 7412–7417, 2018. Available: 10.1109/tap.2018.2872130.
8. Saurabh, A. K. and M. K. Meshram, "Compact sub-6 GHz 5G-multiple-input-multiple-output antenna system with enhanced isolation," *International Journal of RF and Microwave Computer-Aided Engineering*, Vol. 30, No. 8, e22246, 2020.
9. Hei, Y. Q., J. G. He, and W. T. Li, "Wideband decoupled 8-element MIMO antenna for 5G mobile terminal applications," *IEEE Antennas and Wireless Propagation Letters*, Vol. 20, 1448–1452, 2021.
10. Xia, X.-X., Q.-X. Chu, and J.-F. Li, "Design of a compact wideband MIMO antenna for mobile terminals," *Progress In Electromagnetics Research C*, Vol. 41, 163–174, 2013.
11. Sharma, S. and M. Kumar, "Design and analysis of a 4-port MIMO microstrip patch antenna for 5G mid band applications," *Progress In Electromagnetics Research C*, Vol. 129, 231–243, 2023.
12. Wong, K. and Y. Chen, "Small size hybrid loop/open-slot antenna for the LTE smartphone," *IEEE Transactions on Antennas and Propagation*, Vol. 63, No. 12, 5837–5841, 2015. Available: 10.1109/tap.2015.2478960.
13. Biswal, S. P. and S. Das, "Eight-element-based MIMO antenna with CP behaviour for modern wireless communication," *IET Microwaves, Antennas & Propagation*, Vol. 14, No. 1, 45–52, 2020, doi: 10.1049/iet-map.2019.0552.
14. Hazarika, B., B. Basu, and A. Nandi, "Design of antennas using AMC layer to improve gain, flexibility and SAR," *Microwave and Optical Technology Letters*, Vol. 62, No. 12, 3928–3935, 2020.
15. Jiang, W., B. Liu, Y. Cui, and W. Hu, "High-isolation eight-element MIMO array for 5G smartphone applications," *IEEE Access*, Vol. 7, 34104–34112, 2019.
16. Kaur, I., B. Basu, A. K. Singh, V. Rishiwal, S. Tanwar, G. Sharma, P. N. Bokoro, and R. Sharma, "Annular ring ultra-wideband antenna integrated with metallic via array for IoT applications," *IEEE Access*, Vol. 10, 73446–73457, 2022.
17. Kumari, T., G. Das, A. Kumar, and R. K. Gangwar, "Design approach for dual element hybrid MIMO antenna arrangement for wide band application," *International Journal of RF and Microwave Computer-Aided Engineering*, Vol. 29, No. 1, e21486, 2019, https://doi.org/10.1002/mmce.21486.
18. Saurabh, A. K. and M. K. Meshram, "Integration of sub-6 GHz and mm-wave antenna for higher-order 5G-MIMO system," *IEEE Transactions on Circuits and Systems*, Vol. 69, No. 12, 4834–4838, 2022.
19. Sun, L., H. Feng, Y. Li, and Z. Zhang, "Compact 5G MIMO mobile phone antennas with tightly arranged orthogonal-mode pairs," *IEEE Transactions on Antennas and Propagation*, Vol. 66, No. 11, 6364–6369, Nov. 2018.
20. Kumar, D. R., G. V. Babu, K. G. S. Narayan, and N. Raju, "Investigation of 10-port, coupled fed slotted MIMO antenna system for 5G mobile handset," *International Journal of Microwave and Wireless Technologies*, 1–14, 2021.
21. Serghiou, D., M. Khalily, V. Singh, A. Araghi, and R. Tafazolli, "Sub-6 GHz dual band 8×8 MIMO antenna for 5G smartphones," *IEEE Antennas and Wireless Propagation Letters*, Vol. 19, No. 9, 1546–1550, 2020, doi: 10.1109/LAWP.2020.
22. Yang, M. and J. Zhou, "A compact pattern diversity MIMO antenna with enhanced bandwidth and high-isolation characteristics for WLAN/5G/WiFi applications," *Microwave and Optical Technology Letters*, Vol. 62, No. 6, 2353–2364, 2020.
23. Donelli, M. and P. Febvre, "An inexpensive reconfigurable planar array for Wi-Fi applications," *Progress In Electromagnetics Research C*, Vol. 28, 71–81, 2012.

24. Donelli, M., T. Moriyama, and M. Manekiya, "A compact switched-beam planar antenna array for wireless sensors operating at Wi-Fi band," *Progress In Electromagnetics Research C*, Vol. 83, 137–145, 2018.
25. Saputro, S. A., S. Nandiwardhana, and J.-Y. Chung, "Estimation of antenna correlation coefficient of N-port lossy MIMO array," *ETRI Journal*, Vol. 40, No. 3, 303–308, Jun. 2018.
26. Thaysen, J. and K. B. Jakobsen, "Envelope correlation in (N, N) MIMO antenna array from scattering parameters," *Microwave and Optical Technology Letters*, Vol. 48, No. 5, 832–834, 2006.
27. Chae, S. H., W. I. Kawk, S.-O. Park, and K. Lee, "Analysis of mutual coupling in MIMO antenna array by TARC calculation," *2006 Asia-Pacific Microwave Conference*, 2090–2093, Yokohama, Japan, 2006, doi: 10.1109/apmc.2006.4429825.
28. Tausif Afzal Rana, M., M. Arif Khan, W. Afzal, M. Zeeshan Baig, and D. Akhtar, "Effect of scattering parameters on MIMO system capacity," *IOSR Journal of Electrical and Electronics Engineering (IOSR-JEEE)*, Vol. 6, No. 3, 77–81, May–Jun. 2013, www.iosrjournals.org.
29. Chang, L., Y. Yu, K. Wei, and H. Wang, "Polarization-orthogonal co-frequency dual antenna pair suitable for 5G MIMO smartphone with metallic bezels," *IEEE Transactions on Antennas and Propagation*, Vol. 67, 5212–5220, 2019, doi: 10.1109/TAP.2019.2913738.
30. Quddus, A., R. Saleem, T. Shabbir, S. ur Rehman, and M. Farhan Shafique, "Dual port UWB-MIMO antenna with ring decoupling structure," *2016 Progress In Electromagnetic Research Symposium (PIERS)*, 116–119, Shanghai, China, Aug. 8–11, 2016.
31. Jiang, W., B. Liu, Y. Cui, and W. Hu, "High-isolation eight-element MIMO array for 5G smartphone application," *IEEE Access*, Vol. 7, 34104–34112, 2019.
32. Barani, R. R., K.-L. Wong, Y.-X. Zhang, and W.-Y. Li, "Low-profile wideband conjoined open-slot antennas fed by grounded coplanar waveguides for 4×4 5G MIMO operation," *IEEE Transactions on Antennas and Propagation*, Vol. 68, No. 4, 2646–2657, Apr. 2020.
33. Cheng, B. and Z. Du, "A wideband low-profile microstrip MIMO antenna for 5G mobile phones," *IEEE Transactions on Antennas and Propagation*, Vol. 70, No. 2, 1476–1481, Feb. 2022.
34. Cheng, B. and Z. Du, "Dual polarization MIMO antenna for 5G mobile phone applications," *IEEE Transactions on Antennas and Propagation*, Vol. 69, No. 7, 4160–4165, Jul. 2021.
35. Donelli, M., S. K. Menon, G. Marchi, V. Mulloni, and M. Manekiya, "Design of an ultra-wideband antenna based on a SIW resonator," *Progress In Electromagnetic Research C*, Vol. 103, 187–197, 2020.
36. Robol, F. and M. Donelli, "Circularly polarized monopole hook antenna for ISM-band systems," *Microwave and Optical Technology Letters*, Vol. 60, No. 6, 1452–1454, 2018.
37. Viani, F., L. Lizzi, M. Donelli, D. Pregnolato, G. Oliveri, and A. Massa, "Exploitation of parasitic smart antennas in wireless sensor networks," *Journal of Electromagnetic Waves and Applications*, Vol. 24, No. 7, 993–1003, May 1, 2010.
38. Li, Y., Q. Xu, L. Ban, D. Sim, and F. Yu, "Eight-port orthogonally dual-polarised MIMO antennas using loop structures for 5G smartphone," *IET Microwaves, Antennas & Propagation*, Vol. 11, No. 12, 1810–1816, 2017.